Available online at www.sciencedirect.com
SCIENCE DIRECT®
Journal of Computational Physics 205 (2005) 48–71
JOURNAL OF COMPUTATIONAL PHYSICS
www.elsevier.com/locate/jcp

Numerical integration of the three-dimensional Green kernel for an electromagnetic problem ☆

Alexandre Masserey [a], Jacques Rappaz [a], Roland Rozsnyo [a,*], Marek Swierkosz [a,b]

[a] *Institut d'Analyse et de Calcul Scientifique, EPFL, CH-1015 Lausanne, Switzerland*
[b] *Vaudoise Assurances, Lausanne, Switzerland*

Received 17 November 2003; received in revised form 22 June 2004; accepted 21 October 2004
Available online 8 December 2004

Abstract

In this paper, we present a method for the numerical integration of the three-dimensional Green kernel over two triangles. This method is compared with the results obtained by other algorithms. The comparison proves the efficiency of the technique in removing the numerical singularity. Furthermore, we provide a numerical algorithm for increasing the computation accuracy without refining the finite element mesh.

Keywords: Numerical methods; Green kernel; Numerical integration; Boundary element method; Gauss–Hammer quadrature

1. Introduction

This section presents the motivation for integrating the Green Kernel in order to solve an electromagnetic problem in a three-dimensional case. One of the possible applications of the problem is induction heating modeling. Rather than presenting the complete model, which can be found in various papers (see e.g., [1,2,4,5,12–14]), we will focus on the aspects that lead to the integrals we would like to calculate with precision.

☆ Research financed by the Swiss National Fund for Research.
* Corresponding author. Tel.: +41216934234; fax: +41216934303.
E-mail address: roland.rozsnyo@epfl.ch (R. Rozsnyo).

0021-9991/$ - see front matter
doi:10.1016/j.jcp.2004.10.035

1.1. An electromagnetic model for induction heating

Induction heating is used for the thermal treatment of metal pieces in many industrial processes such as brazing, hardening or forging. Inductors in which are flowing alternating currents create a magnetic field which generates eddy currents in the pieces to be treated. The diffusion of the heat due to these currents makes possible the heating process.

Such a problem requires to solve a three-dimensional electromagnetic problem which has been worked out in [1,2,4,12–14]. This model is based on a description of the electromagnetic phenomena inside the conducting pieces and on their borders. The principle of this method consists in taking as unknowns the magnetic field in the conductors and the scalar magnetic potential on the edges of the conductors.

In that model, a so called device for induction heating consists in one or several inductors (current loops) and one or several conductors to be heated (workpieces).

Fig. 1 shows a description of such a system where the inductor is denoted by Ω_i and the conductor by Ω_l. The union of these two open domains is denoted by Ω. The boundary of Ω is Γ ($\Gamma = \partial\Omega$) and the exterior of Ω is Ω_c ($\Omega_c = \mathbb{R}^3 \setminus \bar{\Omega}$). The model requires to introduce two cuts S_i and Σ_i in Ω_i as shown by Fig. 2. The cut S_i has a physical meaning and models the voltage supply, whereas the cut Σ_i appears for theoretical reasons (see [1,2,4,12–14]). Considering the geometry in Fig. 1, we make the following assumptions:

- The frequency of the generator being low enough, we neglect current displacements in Maxwell's equations.
- The various electromagnetic quantities will be written in their time-harmonic form.

With these approximations, Ampère's theorem, Faraday's law and Ohm's law enable writing the following system:

$$\begin{cases} \mathbf{curl}\,\vec{e} + \mathrm{i}\omega\mu\vec{h} = \vec{0} & \text{in } \mathbb{R}^3 \setminus S_i, \\ \mathbf{curl}\,\vec{h} = \sigma\vec{e} & \text{in } \Omega, \\ \mathbf{curl}\,\vec{h} = \vec{0} & \text{in } \Omega_c, \\ [\vec{e} \times \vec{n}]_\Gamma = [\vec{h} \times \vec{n}]_\Gamma = \vec{0} & \text{on } \Gamma, \end{cases} \tag{1}$$

where $\vec{e}$, $\vec{h}$ are, respectively, the electrical and the magnetic field. The quantity σ represents the electrical conductivity and μ the magnetic permeability of materials, ω is the angular frequency of the current. i is

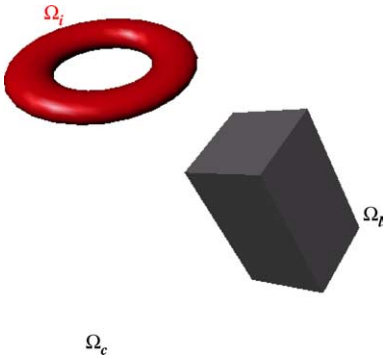

Fig. 1. A device for induction heating.

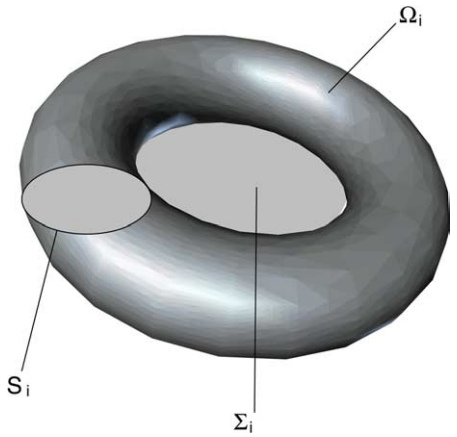

Fig. 2. A model for the inductor.

the imaginary unit number. $[f]_\Gamma$ is the jump of the quantity f on the interface Γ, $\vec{n}$ is the external normal vector to Γ. All the fields are complex valued.

In order to complete this system, we have to add a relation providing the harmonic voltage supply, V, applied to the inductor. This voltage is assumed to be given. We have:

$$\int_c (\vec{e} + \mathrm{i}\omega\vec{a}) \cdot \vec{\tau}\,\mathrm{d}c = V, \tag{2}$$

where $\vec{a}$ is the vector potential defined by $\vec{b} = \mu\vec{h} = \mathbf{curl}\,\vec{a}$ and $\mathbf{div}\,\vec{a} = 0$ in $\mathbb{R}^3$, c is an oriented closed curve in Ω_i, and $\vec{\tau}$ is the unit tangent vector along c.

The system (1) and the Eq. (2) yield the equations to be solved so as to obtain the magnetic field in whole $\mathbb{R}^3$.

1.2. The boundary element method

From Maxwell's equations, a variational formulation of the problem is written in $\Omega\backslash S_i$. After some manipulation, this variational formulation leads in particular to the computation of an integral over Ω_c. Noticing that $\vec{h}$ is vanishing Laplacian in Ω_c, this integral can be decomposed into integrals on the boundary Γ involving the Steklov–Poincaré operator, also known as the Dirichlet–Neumann operator. This idea has been developed in [1] for electromagnetism.

The Steklov–Poincaré operator may be represented in function of two integro-differential operators: the so called simple and double layer potentials. The calculation of these potential yields integrals involving the Green kernel and its normal derivative.

Once the variational formulation has been obtained in the conductors and their edges, one uses a finite element technique to discretize the problem in space. We use a $\mathbb{H}$ (**curl**) [12] finite element method to calculate the magnetic field in Ω and a $\mathbb{P}1$ finite element method to calculate on Γ the potential from which derives the magnetic field. A tetrahedral mesh is used, thus the triangulation of the edges is generated by the trace of the tetrahedrons on them. This method requires the numerical computation of the two integrals involving the Green kernel or its normal derivative over two edge triangles of the mesh. These two triangles may belong either to the same domain or to different ones.

These integrals correspond from the physical point of view to mutual inductances between the different parts of the system. They have their origin in the Biot–Savart law. This law reveals the Green kernel and allows the calculation of the magnetic scalar potential. We present in the next section these two integrals.

1.3. The Green kernel integrals

Our aim is to provide an efficient method for calculating numerically the following integrals,

$$\int_{T_y}\int_{T_x} G(\vec{x},\vec{y})\,\mathrm{d}\Gamma_x\,\mathrm{d}\Gamma_y, \tag{3a}$$

$$\int_{T_y} q^k(\vec{y})\int_{T_x}\frac{\partial G(\vec{x},\vec{y})}{\partial n_x}\,\mathrm{d}\Gamma_x\,\mathrm{d}\Gamma_y, \tag{3b}$$

where $G(\vec{x},\vec{y})$ is the three-dimensional Green kernel defined by $G(\vec{x},\vec{y}) = -\frac{1}{4\pi}\frac{1}{\|\vec{x}-\vec{y}\|}$, $\|.\|$ being the classical euclidean norm, and T_x, T_y are two triangles of $\mathbb{R}^3$. The function $q^k(\vec{y})$, $k = 0,1,2$ is the $\mathbb{P}1$ basis function at the node k of the triangle T_y. The normal vector $\vec{n}_x$ is the unitary normal vector to the triangle T_x, external to the conductor to which T_x belongs. These two integrals are known to be convergent although the integrands are singular. When the two triangles T_x, T_y are far enough from each other, a Gauss–Hammer integration rule provides good results [8]. Nevertheless, when the triangles grow closer and closer (but still distinct), the singularity of the integrands manifests itself and makes the numerical integration blow up. Such a phenomenon has been observed in the case of the numerical simulation of induction heating where the inductor surrounding the workpiece was near the latter. In practice we will be interested in calculating the integrals:

$$I_1 = \int_{T_y}\int_{T_x}\frac{1}{\|\vec{x}-\vec{y}\|}\,\mathrm{d}\Gamma_x\,\mathrm{d}\Gamma_y, \tag{4}$$

and

$$I_2^k = \int_{T_y} q^k(\vec{y})\int_{T_x}\frac{(\vec{x}-\vec{y}).\vec{n}_x}{\|\vec{x}-\vec{y}\|^3}\,\mathrm{d}\Gamma_x\,\mathrm{d}\Gamma_y. \tag{5}$$

It is possible to find various approaches, for instance in [3,9,10], dealing with the numerical integration of a singular kernel over a triangle. However, most of them are not based upon exact integration for removing the singularity. An exact integration method has been developed in [7] and used in [6] in another physical context. This method is using Gauss integral theorems to transform the integration on a given triangle into one integration over the boundary of that triangle. We present here an alternative approach based on finding primitives, which leads to faster computations, as our comparisons will show it, and also to an exact formula in the specific but very important case where the two triangles of integration are overlapped.

2. Reduction of the integration over the reference triangle

2.1. Variable transformation

In order to perform the calculation we introduce the variable transformation u_x that transforms the triangle T_x into the reference triangle, $\hat{T}$, whose nodes A_0, A_1, A_2 have the coordinates $(0,0)$, $(0,1)$, $(1,0)$ in the plane of the new variables (ξ_1, η_1). To define u_x, let's consider the following application:

$$U_x: \quad \hat{T} \to T_x$$
$$(\xi_1,\eta_1) \mapsto U_x(\xi_1,\eta_1) = \sum_{j=0}^{2} u^j(\xi_1,\eta_1)\overrightarrow{OA_j}, \tag{6}$$

where

$$\begin{cases} u^0(\xi_1,\eta_1) = 1 - \xi_1 - \eta_1, \\ u^1(\xi_1,\eta_1) = \xi_1, \\ u^2(\xi_1,\eta_1) = \eta_1. \end{cases} \tag{7}$$

and $\overrightarrow{OA_j}$ is the vector with origin O, the arbitrary origin of $\mathbb{R}^3$, and extremity A_j. Then, $u_x = U_x^{-1}$. In the same way, we define the transformation, u_y that transforms the triangle T_y with nodes B_0, B_1, B_2 into the reference triangle $\hat{T}$ in the plane of the new variables (ξ_2, η_2), as shown in Fig. 3. In our case we have to calculate an integral of the form,

$$I = \int_{T_y}\int_{T_x} F(\vec{x},\vec{y})\,\mathrm{d}\Gamma_x\,\mathrm{d}\Gamma_y, \tag{8}$$

where $F(\vec{x},\vec{y})$ is a locally singular integrand for $\vec{x} = \vec{y}$. Thus, $F(\vec{x},\vec{y})$ is known to be nonsingular when the triangles over which the integration is done are distinct and the integral to be calculated is well defined. However, when T_x and T_y have a non void intersection a numerical singularity appears. If T_x is very close to T_y, then the integrands in (3) are almost singular and numerical integration fails. By making the variable transformations u_x and u_y and defining $f(\xi_1,\eta_1,\xi_2,\eta_2) = F(\vec{x},\vec{y})$, with $\vec{x} = U_x(\xi_1,\eta_1)$ and $\vec{y} = U_y(\xi_2,\eta_2)$, the integral I becomes:

$$I = 4|T_x||T_y| \int_{\hat{T}}\int_{\hat{T}} f(\xi_1,\eta_1,\xi_2,\eta_2)\,\mathrm{d}\xi_1\,\mathrm{d}\eta_1\,\mathrm{d}\xi_2\,\mathrm{d}\eta_2, \tag{9}$$

where $|T|$ is the measure of a given triangle T.

2.2. Numerical calculation of I

A pure numerical calculation of I may be done when $T_x \cap T_y = \emptyset$ by using a N points Gauss–Hammer quadrature formula (see [1]):

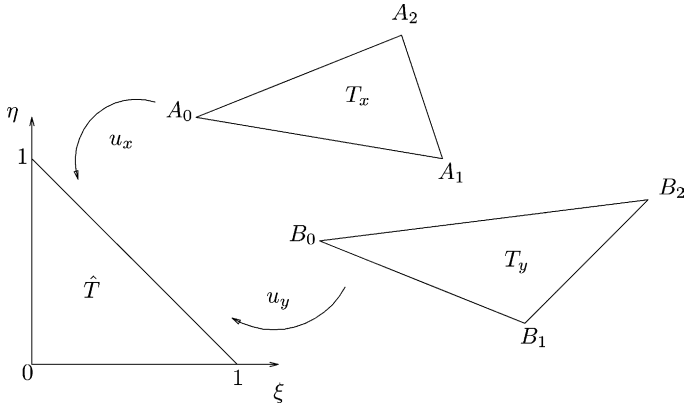

Fig. 3. The transformations u_x and u_y.

$$I \approx 4|T_x||T_y| \sum_{i=1}^{N} \sum_{j=1}^{N} w_i w_j f(\xi^i,\eta^i,\xi^j,\eta^j), \tag{10}$$

where (ξ^i, η^i), are the coordinates of the Gauss–Hammer's points belonging to $\hat{T}$ and w_i, $i = 1,\ldots,N$, are the associated weights. However, when $T_x \cap T_y \neq \emptyset$ or $T_x \cap T_y = \emptyset$ with T_x very close to T_y, this formula leads to difficulties and we suggest another approach to compute I. Let us notice I may be rewritten as:

$$I = 4|T_x||T_y| \int_{\hat{T}} k(\xi_2,\eta_2)\,\mathrm{d}\xi_2\,\mathrm{d}\eta_2, \tag{11}$$

where

$$k(\xi_2,\eta_2) = \int_0^1 \int_0^{1-\eta_1} f(\xi_1,\eta_1,\xi_2,\eta_2)\,\mathrm{d}\xi_1\,\mathrm{d}\eta_1, \tag{12}$$

and

$$f(\xi_1,\eta_1,\xi_2,\eta_2) = \frac{1}{\|U_x(\xi_1,\eta_1) - U_y(\xi_2,\eta_2)\|}, \tag{13}$$

or

$$f(\xi_1,\eta_1,\xi_2,\eta_2) = \frac{(U_x(\xi_1,\eta_1) - U_y(\xi_2,\eta_2)) \cdot \vec{n}_x}{\|U_x(\xi_1,\eta_1) - U_y(\xi_2,\eta_2)\|^3} q^k(\xi_2,\eta_2). \tag{14}$$

The idea is then to calculate exactly $k(\xi_2, \eta_2)$ and to approximate I by a N-points Gauss–Hammer quadrature formula:

$$I \approx 4|T_x||T_y| \sum_{i=1}^{N} w_i k(\xi^i,\eta^i). \tag{15}$$

We will call this method a semi-analytic Gauss–Hammer integration with N points.We show in the following section how $k(\xi_2, \eta_2)$ can be computed as well in the case of I_1 as in the case of I_2^k, $k \in \{0,1,2\}$ (see (4) and (5)).

3. Calculation of $k(\xi_2, \eta_2)$

We now calculate the integral (12) exactly by finding primitives of the kernels defined by (4) and (5) after the reduction to the canonical triangle. Finding these primitives with a software such as Maple is not straightforward. In fact, several cases occur depending on the relative position of the triangles. The properties given here will allow us to identify these different cases and to check that the formulas we will obtain are well defined.

3.1. Some useful properties

We will denote by $\|\cdot\|$ the euclidean norm and by $\overline{AB}$ the distance between two points A and B. We have for any arbitrary origin O and for $M_x \in T_x$, $M_y \in T_y$:

$$\frac{1}{\|\vec{x} - \vec{y}\|} = \frac{1}{\overline{M_x M_y}} = \frac{1}{\sqrt{(\overrightarrow{OM_y} - \overrightarrow{OM_x}) \cdot (\overrightarrow{OM_y} - \overrightarrow{OM_x})}}, \tag{16}$$

$$\frac{(\vec{x}-\vec{y})\cdot\vec{n}_x}{\|\vec{x}-\vec{y}\|^3}=\frac{(\vec{x}-\vec{y})\cdot\vec{n}_x}{\overline{M_xM_y}^3}=\frac{(\overrightarrow{OM_x}-\overrightarrow{OM_y}).\vec{n}_x}{[(\overrightarrow{OM_y}-\overrightarrow{OM_x})\cdot(\overrightarrow{OM_y}-\overrightarrow{OM_x})]^{\frac{3}{2}}}, \tag{17}$$

where $\vec{x}=\overrightarrow{OM_x}$ and $\vec{y}=\overrightarrow{OM_y}$. We also have:

$$\vec{x}=\overrightarrow{OA_0}+\xi_1\overrightarrow{A_0A_1}+\eta_1\overrightarrow{A_0A_2}, \tag{18}$$

$$\vec{y}=\overrightarrow{OB_0}+\xi_2\overrightarrow{B_0B_1}+\eta_2\overrightarrow{B_0B_2}. \tag{19}$$

Defining the following variables:

$$\begin{cases}\beta=\overrightarrow{M_yA_0}\cdot\vec{n}_x,\\ d=\overline{A_0A_1}^2,\\ e=2\overrightarrow{A_0A_1}\cdot\overrightarrow{M_yA_0},\\ g=2\overrightarrow{A_0A_2}\cdot\overrightarrow{A_0A_1},\\ h=\overline{M_yA_0}^2,\\ j=2\overrightarrow{A_0A_2}\cdot\overrightarrow{M_yA_0},\\ k=\overline{A_0A_2}^2,\end{cases} \tag{20}$$

the squared distance $\overline{M_xM_y}^2$ and the scalar product $(\vec{x}-\vec{y})\cdot\vec{n}_x$ may be written in function of the variables ξ_1, η_1 as:

$$\overline{M_xM_y}^2=\mathrm{d}\xi_1^2+e\xi_1+g\xi_1\eta_1+h+j\eta_1+k\eta_1^2, \tag{21}$$

$$(\vec{x}-\vec{y})\cdot\vec{n}_x=\beta. \tag{22}$$

We may then write the five following properties. Most of them are obvious and can be obtained through simple geometrical considerations.

Property 1:

$$j^2-4kh=4\overline{A_0A_2}^2\overline{M_yA_0}^2\left[\cos^2((\overrightarrow{A_0A_2},\overrightarrow{M_yA_0}))-1\right]\leqslant 0. \tag{23}$$

Property 2:

$$(j+g-e-2d)^2-4(d+k-g)(d+h+e)=4\overline{A_1A_2}^2\overline{M_yA_1}^2\left[\cos^2((\overrightarrow{A_1A_2},\overrightarrow{M_yA_1}))-1\right]\leqslant 0. \tag{24}$$

Property 3:

$$g\pm 2\sqrt{dk}=2\overline{A_0A_1A_0A_2}\left[\cos^2(\overrightarrow{A_0A_1},\overrightarrow{A_0A_2})\pm 1\right]\neq 0, \tag{25}$$

because the points A_0, A_1, A_2 are not aligned.
Property 4:

$$(g-2d)\pm 2\sqrt{d(d+k-g)}=2\overline{A_0A_1}\left[\overline{A_0A_2}\cos(\overrightarrow{A_0A_1},\overrightarrow{A_0A_2})-\overline{A_0A_1}\pm\overline{A_1A_2}\right]\neq 0, \tag{26}$$

because the points A_0, A_1, A_2 are not aligned.

Property 5:

$$(2eg-4dj)^2-4(g^2-4dk)(e^2-4dh) = -64\overline{A_0A_1}^4\overline{A_0A_2}^2\overline{M_yA_0}^2\left[\sin^2(\overrightarrow{A_0A_2},\overrightarrow{A_0A_1})\sin^2(\overrightarrow{A_0A_1},\overrightarrow{M_yA_0})\sin^2(\hat{A}_1)\right]\leqslant 0, \tag{27}$$

where $\hat{A}_1$ is the dihedral angle between the two planes defined respectively by the points A_0, A_1, A_2 and A_0, A_1, M_y. We get this equality by using the Gauss relations of the spherical trigonometry.

These five properties will be essential for the following sections.

3.2. Case $F(\vec{x},\vec{y})=\frac{1}{\|\vec{x}-\vec{y}\|}$

We have to distinguish between two situations. The first one is when the point M_y does not belong to the plane $\mathscr{P}_x$ defined by the triangle T_x, the second when it belongs to $\mathscr{P}_x$.

3.2.1. M_y does not belong to $\mathscr{P}_x$

The first integration over ξ_1 corresponding to the relation (12) yields:

$$\begin{aligned}\int_0^{1-\eta_1} f(\xi_1,\eta_1,\xi_2,\eta_2)\,\mathrm{d}\xi_1 &= \frac{\ln((g-2d)\eta_1+e+2d+2\sqrt{\kappa(\eta_1)}\sqrt{d})-\ln(g\eta_1+e+2\sqrt{h+j\eta_1+k\eta_1^2}\sqrt{d})}{\sqrt{d}}\\ &= \frac{\ln(\|\overrightarrow{A_0A_1}\|\|\overrightarrow{M_yA_1}+\eta_1\overrightarrow{A_1A_2}\|+\overrightarrow{A_0A_1}\cdot(\overrightarrow{M_yA_1}+\eta_1\overrightarrow{A_1A_2}))}{\overline{A_0A_1}}\\ &\quad-\frac{\ln(\|\overrightarrow{A_0A_1}\|\|\overrightarrow{M_yA_0}+\eta_1\overrightarrow{A_0A_2}\|+\overrightarrow{A_0A_1}\cdot(\overrightarrow{M_yA_0}+\eta_1\overrightarrow{A_0A_2}))}{\overline{A_0A_1}}\end{aligned} \tag{28}$$

with

$$\kappa(\eta_1)=(h+d+e)+(j+g-e-2d)\eta_1+(d+k-g)\eta_1^2. \tag{29}$$

We shall perform the second integration over η_1 by using two variable changes. Under the assumption that M_y does not belong to $\mathscr{P}_x$, the arguments of the logarithms are always strictly positive for $\eta_1\in[0,1]$. Thus, we have to integrate over that interval two continuous functions of the form $w(\eta_1)=\ln(A\eta_1+B+K\sqrt{C\eta_1^2+D\eta_1+E})$, where C is a positive number and where $\Delta=D^2-4CE<0$, according to properties 1 and 2 with M_y not belonging to $\mathscr{P}_x$. We have:

$$w(\eta_1)=\ln\left(A\eta_1+B+K\sqrt{C}\sqrt{\left(\eta_1+\frac{D}{2C}\right)^2-\frac{\Delta}{4C^2}}\right). \tag{30}$$

Performing the first change of variable $t=\eta_1+\frac{D}{2C}$, we obtain:

$$\int_0^1 w(\eta_1)\,\mathrm{d}\eta_1=\int_{\frac{D}{2C}}^{1+\frac{D}{2C}}\ln\left(At-\frac{AD}{2C}+B+K\sqrt{C}\sqrt{t^2-\frac{\Delta}{4C^2}}\right)\mathrm{d}t. \tag{31}$$

The second change of variable is $t = \sqrt{-\frac{\Delta}{4C^2}}\sinh(u)$. Thus,

$$\int_0^1 w(\eta_1)\,\mathrm{d}\eta_1 = \sqrt{-\frac{\Delta}{4C^2}} \int_{\operatorname{arcsinh}\left(\frac{D}{2C}\sqrt{-\frac{4C^2}{\Delta}}\right)}^{\operatorname{arcsinh}\left(\left(1+\frac{D}{2C}\right)\sqrt{-\frac{4C^2}{\Delta}}\right)} \times \ln\left(A\sqrt{-\frac{\Delta}{4C^2}}\sinh(u) - \frac{AD}{2C} + B + K\sqrt{-\frac{\Delta}{4C}}\cosh(u)\right)\cosh(u)\,\mathrm{d}u. \tag{32}$$

We then have to integrate a function of the form $\tilde{w}(u) = \ln(U\cosh(u) + V\sinh(u) + Z)\cosh(u)$, where U, V, Z are real constants with respect to the integration. A primitive of such a function is given by:

$$\begin{aligned}\int \tilde{w}(u)\,\mathrm{d}u = {} & \frac{\left(VZ - U\sqrt{Z^2+V^2-U^2}\right)\ln\left(e^u + \frac{\sqrt{Z^2+V^2-U^2}+Z}{(V+U)}\right)}{V^2-U^2} \\ & + \frac{\left(U\sqrt{Z^2+V^2-U^2} + VZ\right)\ln\left(e^u + \frac{-\sqrt{Z^2+V^2-U^2}+Z}{(V+U)}\right)}{V^2-U^2} - \frac{Zu}{V-U} \\ & + \sinh(u)[\ln(U\cosh(u) + V\sinh(u) + Z) - 1].\end{aligned} \tag{33}$$

According to properties 3 and 4, we may check that $V \pm U \neq 0$. Although this formula has to be used when M_y does not belong to $\mathscr{P}_x$, it works in the particular case where M_y belongs to $\mathscr{P}_x$ and lies inside the triangle A_0, A_1, A_2, out of the edges. Then, the expression (28) is well defined (no logarithm of zero).

3.2.2. M_y belongs to $\mathscr{P}_x$

Let us consider first the integrals

$$K_i(\vec{y}) = \int_{T_x^i} F(\vec{x},\vec{y})\,\mathrm{d}\Gamma_x, \quad K(\vec{y}) = \int_{T_x} F(\vec{x},\vec{y})\,\mathrm{d}\Gamma_x, \tag{34}$$

where the vertices of triangle T_x^i are the points M_y, A_i, A_{i+1}, $i \in \{0,1,2\}$, the sums being taken modulo 3. Performing the first change of variables defined by, $\vec{x} = (1-\xi_1-\eta_1)\overrightarrow{OA_i} + \xi_1\overrightarrow{OM_y} + \eta_1\overrightarrow{OA_{i+1}}$, we obtain

$$K_i(\vec{y}) = 2|T_x^i| n t_{\hat{T}} \frac{\mathrm{d}\xi_1 \mathrm{d}\eta_1}{\|(1-\xi_1)\vec{v}_i - \eta_1\vec{a}_i\|}, \tag{35}$$

with $\vec{v}_i = \overrightarrow{M_yA_i}$ and $\vec{a}_i = \overrightarrow{A_{i+1}A_i}$. Making then the second change of variables $\xi_1 = s$, $\eta_1 = (1-s)t$, we get:

$$K_i(\vec{y}) = 2|T_x^i| \int_0^1 \frac{\mathrm{d}t}{\|\vec{v}_i - t\vec{a}_i\|} = 2|T_x^i| \int_0^1 \frac{\mathrm{d}t}{\sqrt{\|\vec{a}_i\|^2 t^2 - 2\vec{v}_i\cdot\vec{a}_i t + \|\vec{v}_i\|^2}}. \tag{36}$$

The calculation of that integral gives:

$$K_i(\vec{y}) = 2\frac{|T_x^i|}{\|\vec{a}_i\|}(\ln((\vec{a}_i - \vec{v}_i)\cdot\vec{a}_i + \|\vec{a}_i - \vec{v}_i\|\|\vec{a}_i\|) - \ln(\|\vec{a}_i\|\|\vec{v}_i\| - \vec{v}_i\cdot\vec{a}_i)). \tag{37}$$

It is easy to check that this formula is always well defined under our assumptions provided that the triangle T_x^i is not degenerate. However, if it is the case $|T_x^i| = 0$ and $K_i(\vec{y}) = 0$.

At that stage, we may notice that it is always possible to express the domain T_x as a combination of the domains T_x^0, T_x^1, T_x^2 such that $K(\vec{y}) = \epsilon_0 K_0(\vec{y}) + \epsilon_1 K_1(\vec{y}) + \epsilon_2 K_2(\vec{y})$, where $\epsilon_i = \pm 1$, $i \in \{0,1,2\}$ an example is given by the Fig. 4.

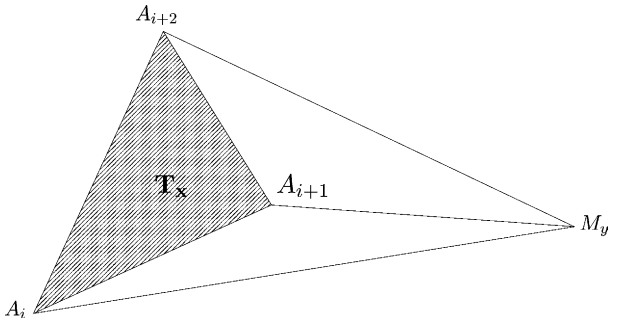

Fig. 4. An example of configuration where $|T_x| = |T_x^{i+2}| - |T_x^{i+1}| - |T_x^i|$.

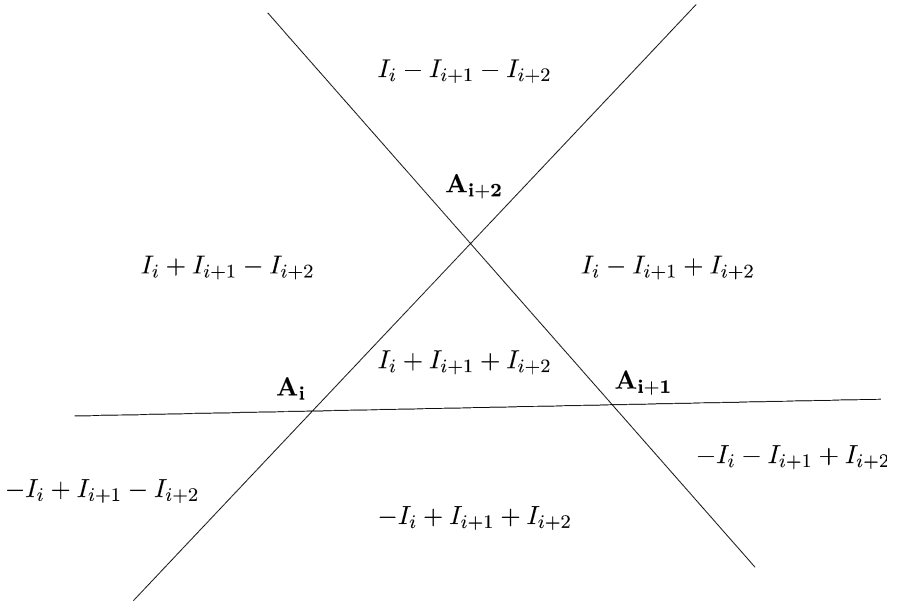

Fig. 5. Value of I in function of I_i, I_{i+1} and I_{i+2} depending on the region to which M_y belongs. At the interfaces, one or two integrals from I_i, I_{i+1} and I_{i+2} vanish.

The values of the ϵ_i are the same as in the unique combination from seven possible ones that gives the area of the triangle T_x in function of the measures of the triangles T_x^i, as shown by the Fig. 5: $|T_x| = \epsilon_0|T_x^0| + \epsilon_1|T_x^1| + \epsilon_2|T_x^2|$.

If we consider $I_i = \int_{T_y} K_i(\vec{y})\,\mathrm{d}\Gamma_y$, I_i is numerically computed by

$$I_i \approx 2|T_y| \sum_{j=1}^{N} w_j K_i(U_y(\xi_2^j, \eta_2^j)).$$

Then, $I \approx \epsilon_0 I_0 + \epsilon_1 I_1 + \epsilon_2 I_2$.

3.2.3. The particular case when T_x and T_y are the same triangles

In that case, it is possible to obtain an exact formula for I. The point M_y belongs to the triangle T_x as shown by the Fig. 6 and we have $I = \sum_{i=0}^{2} \int_{T_y} K_i(\vec{y})\,\mathrm{d}\Gamma_y$. Using the relation (37), we split this integral in two parts:

$$I = \sum_{i=0}^{2} (E_2^i - E_1^i), \tag{38}$$

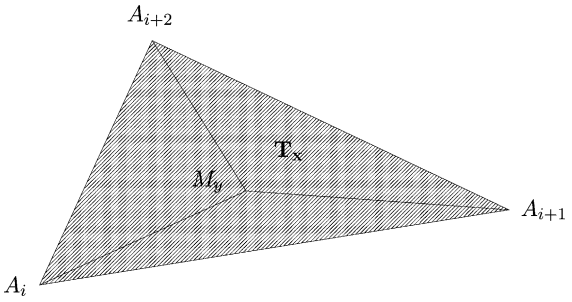

Fig. 6. Situation when T_x and T_y are the same.

with

$$E_2^i = \int_{T_y} 2\frac{|T_x^i|}{\|\vec{a}_i\|} \ln\left((\vec{a}_i - \vec{v}_i)\cdot\vec{a}_i + \|\vec{a}_i - \vec{v}_i\|\|\vec{a}_i\|\right) \mathrm{d}\Gamma_y, \tag{39}$$

and

$$E_1^i = \int_{T_y} 2\frac{|T_x^i|}{\|\vec{a}_i\|} \ln\left(\|\vec{a}_i\|\|\vec{v}_i\| - \vec{v}_i\cdot\vec{a}_i\right) \mathrm{d}\Gamma_y. \tag{40}$$

Where we consider E_2^i, we perform successively the two changes of variables defined by: $\vec{y} = (1-\xi_1-\eta_1)\overrightarrow{OA_i} + \xi_1\overrightarrow{OA_{i+1}} + \eta_1\overrightarrow{OA_{i+2}}$ and $\xi_1 = s$, $\eta_1 = (1-s)t$, which gives $\vec{a}_i - \vec{v}_i = (1-s)(\vec{a}_i + t\vec{a}_{i+2})$ and $2|T_x^i| = 2(1-s)t|T_x|$. We obtain:

$$E_2^i = 4\frac{|T_x|^2}{\|\vec{a}_i\|}\int_{\tilde{T}} (1-s)^2 t \ln(1-s)\left((\vec{a}_i + t\vec{a}_{i+2})\cdot\vec{a}_i + \|\vec{a}_i + t\vec{a}_{i+2}\|\|\vec{a}_i\|\right) \mathrm{d}s\,\mathrm{d}t, \tag{41}$$

where $\tilde{T}$ is the unit square in the plane (s, t). The integration gives:

$$E_2^i = 4\frac{|T_x|^2}{\|\vec{a}_i\|}\left(-\frac{5}{36} + \frac{\|\vec{a}_i\|(\|\vec{a}_{i+1}\| - \|\vec{a}_i\|)}{6\|\vec{a}_{i+2}\|^2} + \frac{1}{6}\ln(\|\vec{a}_{i+1}\|\|\vec{a}_i\| + \|\vec{a}_i\|^2 + \vec{a}_i\cdot\vec{a}_{i+2}) + \frac{\|\vec{a}_i\|\vec{a}_i\cdot\vec{a}_{i+2}}{6\|\vec{a}_i\|^3}\ln\left(\frac{\|\vec{a}_i\|\|\vec{a}_{i+2}\| + \vec{a}_i\cdot\vec{a}_{i+2}}{\|\vec{a}_{i+1}\|\|\vec{a}_{i+2}\| + \|\vec{a}_{i+2}\|^2 + \vec{a}_i\cdot\vec{a}_{i+2}}\right)\right). \tag{42}$$

Where we consider E_1^i, we perform successively the two changes of variables defined by: $\vec{y} = (1-\xi_1-\eta_1)\overrightarrow{OA_{i+1}} + \xi_1\overrightarrow{OA_i} + \eta_1\overrightarrow{OA_{i+2}}$ and $\xi_1 = s$, $\eta_1 = (1-s)t$, which gives $\vec{v}_i = (1-s)(\vec{a}_i + t\vec{a}_{i+1})$ and $2|T_x^i| = 2(1-s)t|T_x|$. We obtain:

$$E_1^i = 4\frac{|T_x|^2}{\|\vec{a}_i\|}\int_{\tilde{T}} (1-s)^2 t \ln(1-s)\left(\|\vec{a}_i + t\vec{a}_{i+1}\|\|\vec{a}_i\| - (\vec{a}_i + t\vec{a}_{i+1})\cdot\vec{a}_i\right) \mathrm{d}s\,\mathrm{d}t. \tag{43}$$

The integration gives:

$$E_1^i = 4\frac{|T_x|^2}{\|\vec{a}_i\|}\left(-\frac{5}{36} + \frac{\|\vec{a}_i\|(\|\vec{a}_i\| - \|\vec{a}_{i+2}\|)}{6\|\vec{a}_{i+2}\|^2} + \frac{1}{6}\ln(\|\vec{a}_{i+2}\|\|\vec{a}_i\| - \|\vec{a}_i\|^2 - \vec{a}_i\cdot\vec{a}_{i+1}) + \frac{\|\vec{a}_i\|\vec{a}_i\cdot\vec{a}_{i+1}}{6\|\vec{a}_{i+1}\|^3}\ln\left(\frac{\|\vec{a}_{i+1}\|\|\vec{a}_{i+2}\| + \|\vec{a}_{i+1}\|^2 + \vec{a}_i\cdot\vec{a}_{i+1}}{\|\vec{a}_i\|\|\vec{a}_{i+1}\| + \vec{a}_i\cdot\vec{a}_{i+1}}\right)\right). \tag{44}$$

Summing over i, we get the final formula:

$$I = \frac{2}{3}|T_x|^2 \sum_{(i,j,k)\in\mathscr{F}} \left(\frac{n_i^2 - p_{ik}}{n_i^3} \ln(p_{ik} + n_i^2 + n_i n_j) - \frac{1}{n_i} \ln(-p_{ij} - n_i^2 + n_i n_k) + p_{jk}\left(\frac{1}{n_j^3} + \frac{1}{n_k^3}\right) \ln(p_{jk} + n_j n_k) - \frac{p_{ij}}{n_i^3} \ln(p_{ij} + n_i^2 + n_i n_k) \right), \tag{45}$$

where: $\mathscr{F} = \{(0,1,2);(1,2,0);(2,0,1)\}$, $n_i = \|\vec{a}_i\|$ and $p_{ij} = \vec{a}_i \cdot \vec{a}_j$.

3.3. Case $F(\vec{x},\vec{y}) = \frac{(\vec{x}-\vec{y})\cdot\vec{n}_x}{\|\vec{x}-\vec{y}\|^3} q^k(\vec{y})$

We have to calculate the integral:

$$\int_0^1 \int_0^{1-\eta_1} f(\xi_1,\eta_1,\xi_2,\eta_2)\,\mathrm{d}\xi_1\,\mathrm{d}\eta_1 = \int_0^1 \int_0^{1-\eta_1} \frac{\beta q^k(\xi_2,\eta_2)}{(\mathrm{d}\xi_1^2 + e\xi_1 + g\xi_1\eta_1 + h + j\eta_1 + k\eta_1^2)^{\frac{3}{2}}}\,\mathrm{d}\xi_1\,\mathrm{d}\eta_1, \tag{46}$$

The function $q^k(\xi_2, \eta_2)$ is constant with respect to (ξ_1,η_1); it is not restrictive to consider $q^k = 1$. Then, we split the integration in two parts such that:

$$\int_0^{1-\eta_1} \frac{\beta}{(\mathrm{d}\xi_1^2 + e\xi_1 + g\xi_1\eta_1 + h + j\eta_1 + k\eta_1^2)^{\frac{3}{2}}}\,\mathrm{d}\xi_1 = Q_1 + Q_2, \tag{47}$$

where

$$Q_1 = 2\frac{\beta(2d-g)\eta_1 - \beta(2d+e)}{z(\eta_1)\sqrt{(d+k-g)\eta_1^2 + (g+j-e-2d)\eta_1 + e + d + h}}, \tag{48}$$

$$Q_2 = 2\frac{\beta g\eta_1 + \beta e}{z(\eta_1)\sqrt{k\eta_1^2 + j\eta_1 + h}}, \tag{49}$$

with

$$z(\eta_1) = \left(g^2 - 4dk\right)\eta_1^2 + (-4dj + 2eg)\eta_1 + e^2 - 4dh. \tag{50}$$

In order to perform the second integration we are led to find the integral of a function of the form:

$$w(\eta_1) = \frac{b\eta_1 + c}{(n\eta_1^2 + l\eta_1 + m)\sqrt{r\eta_1^2 + s\eta_1 + t}}. \tag{51}$$

We may consider a classification based upon several cases induced by the values of the quantities $s^2 - 4rt$, the discriminant of $r\eta_1^2 + s\eta_1 + t$ and $l^2 - 4nm$, the discriminant of $n\eta_1^2 + l\eta_1 + m$, in relation with the properties 1, 2 and 5.

3.3.1. Case 1: $s^2 - 4rt = 0$

When this case occurs, it means according to properties 1 and 2 that M_y belongs to the plane defined by the points A_0, A_1, A_2. Then, the coefficient β in (48) and (49) is zero and $Q_1 = Q_2 = 0$. Thus:

$$\int_0^1 w(\eta_1)\,\mathrm{d}\eta_1 = 0. \tag{52}$$

3.3.2. Case 2: $s^2-4rt < 0$

In order to perform the exact integration in this case let us first explicit ζ and ς, the roots of the equation $n\eta_1^2 + l\eta_1 + m = 0$, and two other related quantities, ϕ and ψ:

$$\zeta = \frac{-l - \sqrt{l^2 - 4nm}}{2n}, \tag{53}$$

$$\varsigma = \frac{-l + \sqrt{l^2 - 4nm}}{2n}, \tag{54}$$

$$\phi = \sqrt{2(r\varsigma^2 + s\varsigma + t)}, \tag{55}$$

$$\psi = \sqrt{2(r\zeta^2 + s\zeta + t)}. \tag{56}$$

subcase 1: $l^2 - 4nm = 0$

According to property 5, this means that M_y belongs to $\mathscr{P}_x$. Then, like previously, the coefficient β in (48) and (49) is equal to zero and $Q_1 = Q_2 = 0$. Thus:

$$\int_0^1 w(\eta_1)\,\mathrm{d}\eta_1 = 0. \tag{57}$$

subcase 2: $l^2 - 4nm < 0$, $\phi \neq 0$ and $\psi \neq 0$

Then, ζ and $\varsigma$are the complex conjugated roots of $n\eta_1^2 + l\eta_1 + m = 0$ but are not the roots of $r\eta_1^2 + s\eta_1 + t = 0$. Using Maple we get a primitive of w:

$$\int w(\eta_1)\,\mathrm{d}\eta_1 = \sqrt{2}\frac{\ln\left(\frac{\psi^2+(s+2r\zeta)(\eta_1-\zeta)+\sqrt{2}\psi\sqrt{r\eta_1^2+s\eta_1+t}}{\eta_1-\zeta}\right)(b\zeta+c)}{n(\varsigma-\zeta)\psi} - \sqrt{2}\frac{\ln\left(\frac{\phi^2+(s+2r\varsigma)(\eta_1-\varsigma)+\sqrt{2}\phi\sqrt{r\eta_1^2+s\eta_1+t}}{\eta_1-\varsigma}\right)(b\varsigma+c)}{n(\varsigma-\zeta)\phi}. \tag{58}$$

We may check under our assumptions that this expression is well defined (no divisions by zero) for $\eta_1 \in [0,1]$. We have the difference of two complex quantities, which gives a real value after combining the conjugated expressions.

subcase 3: $l^2 - 4nm < 0$, $\phi = 0$ and $\psi = 0$

The assumptions of the present subcase mean that ζ and $\varsigma$are not only the complex conjugated roots of $n\eta_1^2 + l\eta_1 + m$, but also the complex conjugated roots of $r\eta_1^2 + s\eta_1 + t$. Thus, the expression (51) has to be rewritten as:

$$w(\eta_1) = \frac{1}{n\sqrt{r}}\frac{b\eta_1 + c}{(\eta_1^2 - S\eta_1 + P)^{\frac{3}{2}}}, \tag{59}$$

where $S = \zeta + \bar{\zeta}$ and $P = \zeta\bar{\zeta}$. A primitive of w is then given by:

$$\int w(\eta_1)\,\mathrm{d}\eta_1 = \frac{2}{n\sqrt{r}}\frac{-(bS + 2c)\eta_1 + cS + 2bP}{(S^2 - 4P)\sqrt{\eta_1^2 - S\eta_1 + P}}. \tag{60}$$

This formula is always well defined in that case because $n \neq 0$, $r \neq 0$ and $S^2 - 4P < 0$, which implies $\eta_1^2 - S\eta_1 + P > 0$ for any $\eta_1 \in [0,1]$.

3.4. Conclusion of this section

We were led to consider several cases in order to perform an exact integration to find $k(\xi_2, \eta_2)$ for the computation of I_1 and I_2^k. In each one we gave the formula to be used. These formulas have no more numerical singularities and may be integrated safely by a Gauss–Hammer quadrature rule.

4. Comparisons between numerical and semi-analytic Gauss–Hammer integration

In this section, we make numerical experiments with the geometrical configuration presented by the Fig. 7. In that case the triangles T_x and T_y have the same shape and lie in two distinct parallel planes, one triangle over an other such that the distance between these two triangles may be defined as the distance between these planes. When the distance decreases to zero, the overlapping of the triangles becomes maximal so that the numerical singularities should be extreme. Let h be the distance between the two triangles and a_0 be the parameter defined in the next section. We compare the calculation of the integrals of kind I_1 and I_2^0 versus the dimensionless variable h/a_0 by different numerical methods and show the improvement obtained by the semi-analytical Gauss–Hammer integration in removing the numerical singularity. Details about the other numerical methods are available in references [8,11]. We also give calculation time cost comparisons.

4.1. Comparisons between different numerical methods

We compare the following methods in order to compute numerically I of the relation (15): Gauss–Hammer quadrature formula with $N = 3$ points (GH_3) and $N = 9$ points (GH_9), adaptive double

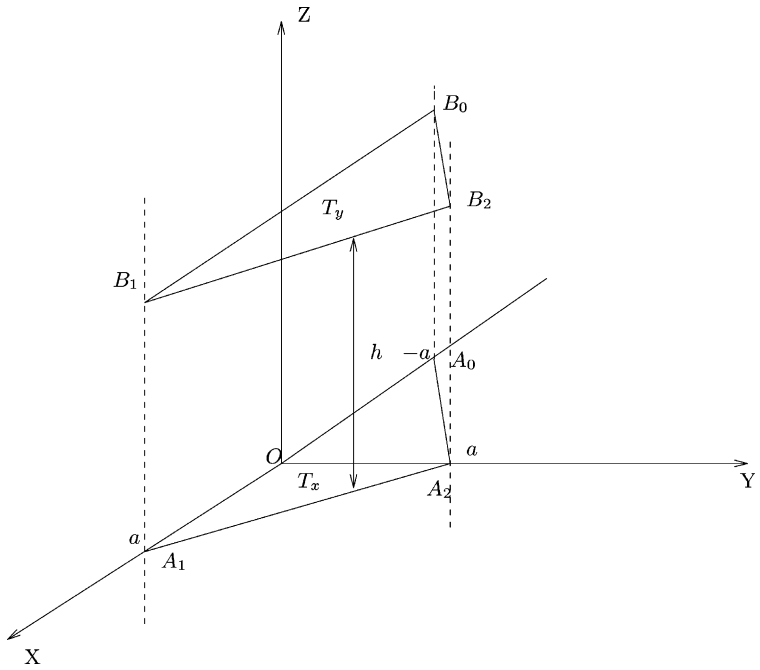

Fig. 7. The configuration of T_x and T_y for numerical experiments.

exponential quadrature (ADEXP), semi-analytic Gauss–Hammer quadrature formula with $N = 3$ points ($SAGH_3$) and $N = 9$ points ($SAGH_9$), the exact integration method used in [6,7], based on boundary integration (EBI).

We chose as a reference for comparisons two methods: a method using the one-dimensional adaptive double exponential quadrature, because it is known to handle very well the kernels having local removable singularities (see for instance [11] for the double exponential transformation in numerical analysis), and EBI an alternative exact integration method from which we should get the same results. However, unlike in [6] where the numerical integration over the second triangle is done by the use of one-dimensional quadrature formulas, we combine the use of EBI with the two-dimensional Gauss–Hammer quadrature formulas with $N = 9$ points (EBI_9) for the integration over that second triangle.

We apply the double exponential algorithm to the exact formula obtained by the first integration in (12), this formula still not removing the numerical singularities. We required ten digits of precision in order to compute this integral with accuracy, the second double integration being performed by a Gauss–Hammer rule with $N = 9$ points.

The results comparing all the methods except EBI_9 are presented on Fig. 8 for I_1 and Fig. 9 for I_2^0 (see (4) and (5) for the definition). In both cases the upper graph is a zoom of the lower one. Fig. 10 is devoted to the comparison between $SAGH_9$ and EBI_9 for the computation of I_0 and I_2^0. For these comparisons the coordinates of the points corresponding to the corners of the two triangles are: $A_0(-a,0,0)$, $A_1(a,0,0)$, $A_2(0,a,0)$, $B_0(-a,0,h)$, $B_1(a,0,h)$, $B_2(0,a,h)$. We took $a = a_0 = 5 \times 10^{-3}$. The dimensionless ratio h/a_0 varies in the interval $[2 \times 10^{-4},2]$.

Figs. 8 and 9 show that the semi-analytical method does not blow up when h/a_0 tends to zero and gives values in accordance with those obtained by the adaptive double exponential quadrature, whereas the pure numerical Gauss–Hammer method is diverging when h/a_0 tends to zero. However, we can see that for the two kinds of integrals, I_1 and I_2^0, the various methods give similar values when h/a_0 is greater than 1, for that particular geometrical configuration.

In addition, it is possible to check that I_1 converges to the value calculated by the exact formula for overlapped triangles, i.e., $I_1(0) = 3.5611 \times 10^{-7}$ when h/a_0 tends to zero, and that I_2^0 converges to zero when h/a_0 tends to zero, as it is indicated by the the definition of this integral.

To compare $SAGH_9$ with EBI_9, we implemented the formulas given in the appendix of [6]. Fig. 10 shows that the results obtained by $SAGH_9$ and EBI_9 are the same, as expected.

These two integrals are functions of the parameter a and the distance h, such that we may write $I_1 = I_1(a,h)$ and $I_2^0 = I_2^0(a,h)$. If we want to deduce their values for any couple (a, h) from the values calculated with (a_0, h), we may use the following properties:

$$\begin{cases} I_1(\lambda a,\lambda h) = \lambda^3 I_1(a,h), & I_1(\lambda a,h) = \lambda^3 I_1(a,\frac{h}{\lambda}), \\ I_2^0(\lambda a,\lambda h) = \lambda^2 I_2^0(a,h), & I_2^0(\lambda a,h) = \lambda^2 I_2^0(a,\frac{h}{\lambda}), \end{cases} \tag{61}$$

where λ is a strictly positive factor. Thus, if we want to know the values of these integrals for a given ratio h/a, we have to multiply the values given by Fig. 8 by the conversion factor λ to the power 3 and the values given by Fig. 9 by the conversion factor λ to the power 2.

Examining the time cost related with these two methods, we notice that the ratio between a Gauss–Hammer quadrature method with $N = 3$ points and $N = 9$ points is about 9, which corresponds to the ratio of the number of loops for computation between the two methods. The same thing holds for the semi-analytic Gauss–Hammer method.

The adaptive double exponential quadrature method ([11]) is very expensive in time, in particular because ten digits of precision were required in order to approximate with a good accuracy the exact value obtained for the integral over T_x.

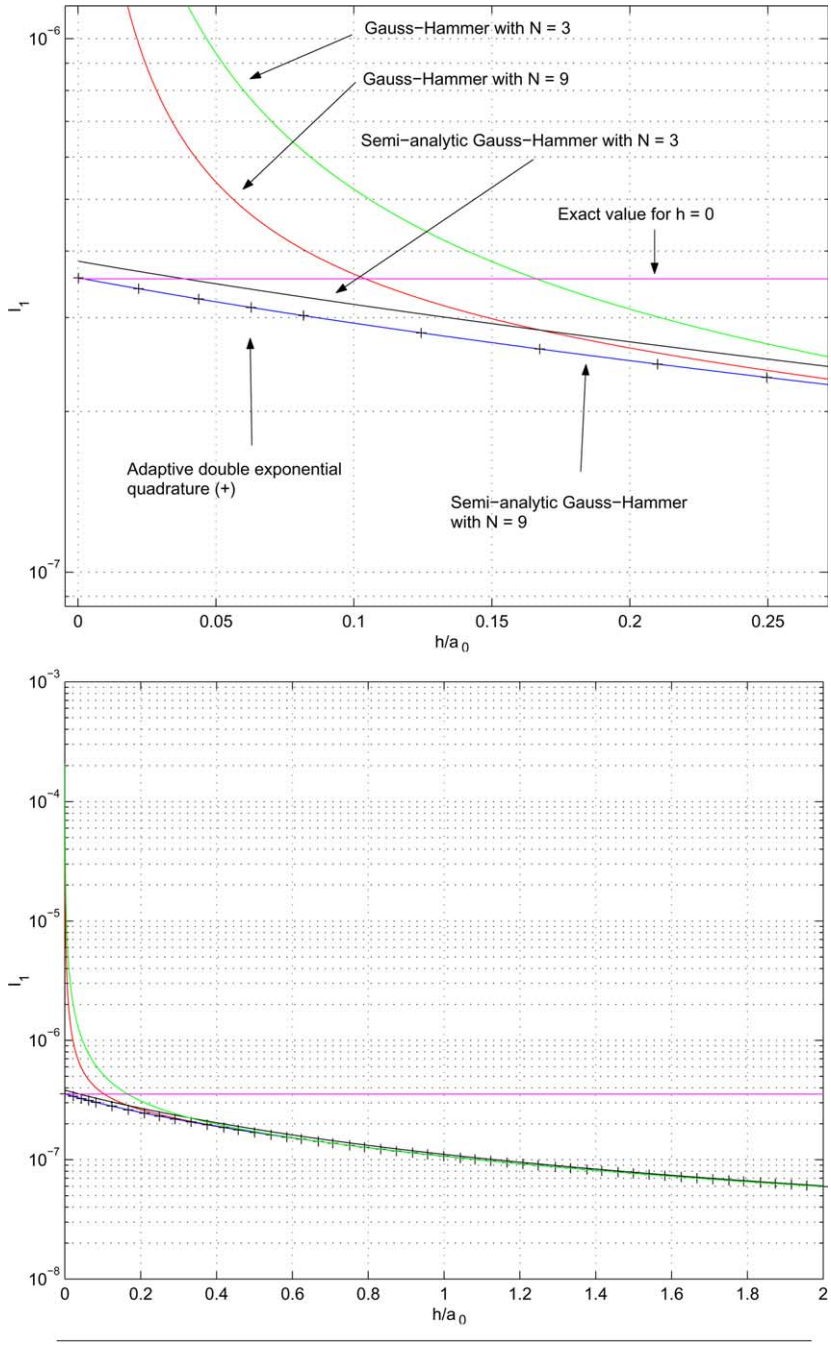

Numerical Method	GH_3	GH_9	$SAGH_3$	$SAGH_9$	$ADEXP$
Relative Time Cost	1	8.65	3.95	12.1	1700

Fig. 8. Comparisons between different numerical methods and relative associated time costs for I_1.

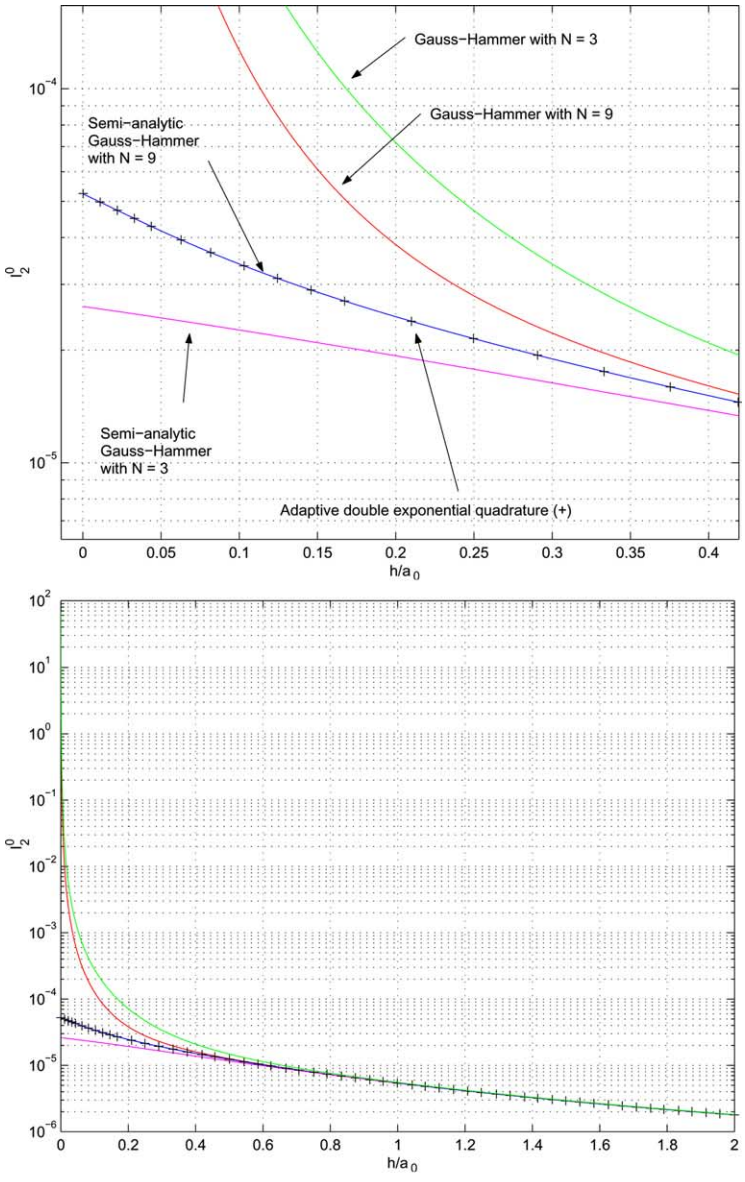

Numerical Method	GH_3	GH_9	$SAGH_3$	$SAGH_9$	$ADEXP$
Relative Time Cost	1	8.65	2.15	6.65	2238

Fig. 9. Comparisons between different numerical methods and relative associated time costs for I_2^0.

Comparing the time costs between semi-analytic and pure Gauss–Hammer methods, we can see for I_2^0, with $N = 9$ points, the semi-analytic Gauss–Hammer method is 23% faster than a pure Gauss–Hammer method, whereas it is 40% slower in the case of I_1.

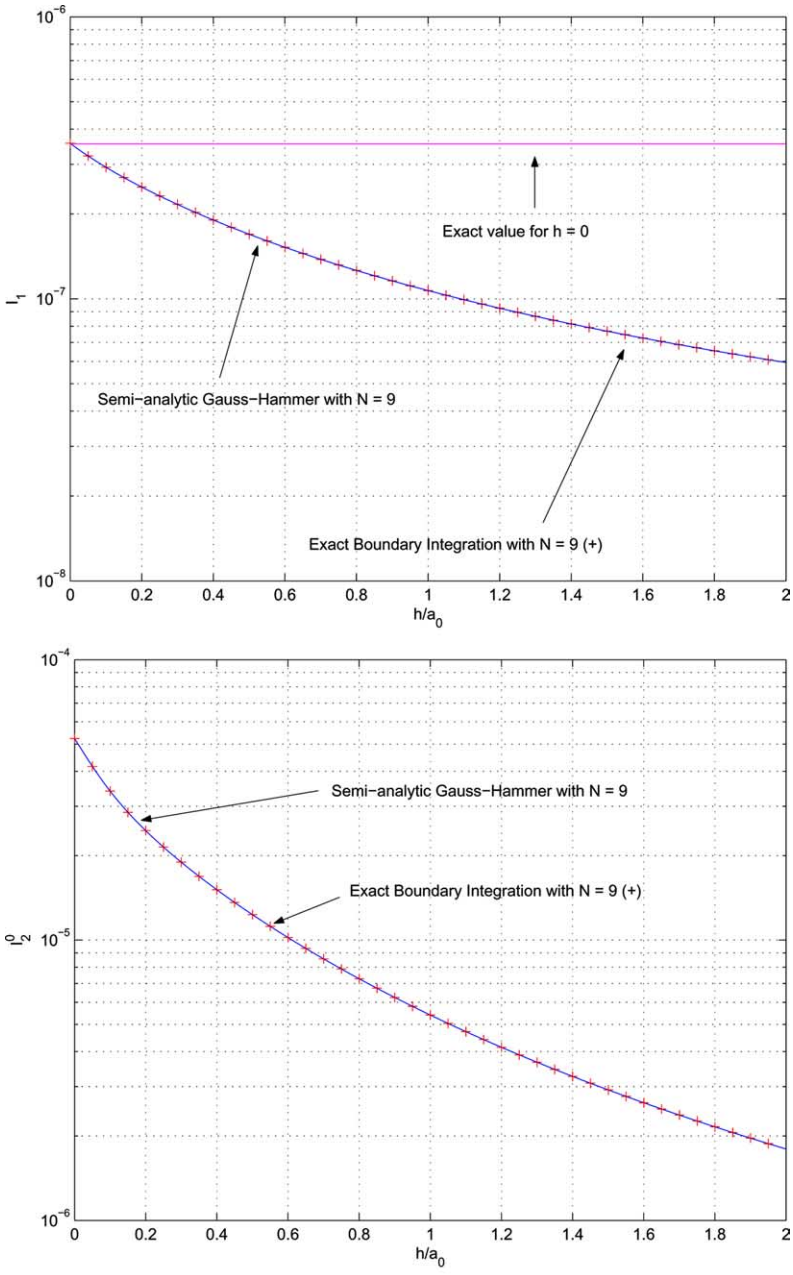

Numerical Method	$SAGH_9$	EBI_9
Relative Time Cost for I_0	1	3.4
Relative Time Cost for I_2^0	1	4.5

Fig. 10. Comparisons between $SAGH_9$ and EBI_9 for the computation of I_0 and I_2^0 and relative associated time costs.

Comparing now $SAGH_9$ with EBI_9, we get that $SAGH_9$ is 3.4 times faster for the computation of I_0 and 4.5 times faster for the computation of I_2^0. This can be explained by the differences between the formulas obtained in the two methods even if they give the same results.

The time cost of the semi-analytic Gauss–Hammer method is related to the complexity of the formula obtained by exact integration. However, the semi-analytic method reduces considerably the calculation time when the computation of the exact formula becomes faster than the computation of the nested sum of the pure numerical integration, which happens when the number of quadrature points is increased.

In practice, we would like to perform our computations using the fastest and the most accurate method. In a general configuration of the triangles, there are no exact formulas to compare with numerical calculations. However, the semi-analytical Gauss–Hammer quadrature method improves the computation error by removing the numerical singularity and cancelling one quadrature rule, with a computation time of the same order compared to the pure quadrature methods we tested. But this improvement may not be satisfactory. Thus, we present in the sequel a method allowing to obtain a better accuracy of the computation.

5. Improvement of the computation accuracy

In the previous sections, we have shown how it was possible to remove the singularities in the numerical integrations by using partial exact integrations. After the exact integration there is still a pure numerical one to be computed. The resulting error is not known in the three-dimensional case unlike in the one-dimensional one where error estimations exist. Due to the lack of an exact formula enabling comparisons, except when the two integration triangles are the same, we are led to chose an algorithmic method for efficient computation. Inspired by the one-dimensional case, we have chosen to keep the number of Gauss–Hammer points constant. It is well known in the case of the numerical integration of a one-dimensional singular kernel that it is better to increase the number of integration intervals rather than the number of Gauss–Legendre points to achieve a given precision. Thus, the number of quadrature points was fixed to $N = 9$ and the integration triangle was subdivided into sub-triangles in a particular manner. We describe in this chapter this subdivision algorithm allowing to increase the precision. To show the efficiency of the method we make a comparison in the case where the two triangles of integration are the same for the integration of the Green kernel, the only case for which we have an exact formula.

5.1. Decomposition of the integration by subdivision of the triangle $\hat{T}$

We explain here how we subdivide the reference triangle to decompose the integration. Fig. 11 shows the subdivision method for the first step.

Let us consider the integration of a continuous function k over the reference triangle $\hat{T}$. If we denote by T_A the triangle determined by the points $O(0,0)$, $A(0,1)$, $J(\frac{1}{2},\frac{1}{2})$ and by T_B the triangle determined by the points $O(0,0)$, $B(1,0)$, $J(\frac{1}{2},\frac{1}{2})$, we may write:

$$K = \int_{\hat{T}} k(\xi,\eta)\,\mathrm{d}\xi\,\mathrm{d}\eta = \int_{T_A} k(\xi,\eta)\,\mathrm{d}\xi\,\mathrm{d}\eta + \int_{T_B} k(\xi,\eta)\,\mathrm{d}\xi\,\mathrm{d}\eta. \tag{62}$$

Considering the mappings

$$\begin{aligned} &U_A : \hat{T} \to T_A \\ &\quad (\xi',\eta') \mapsto U_A(\xi',\eta') = Ju^0(\xi',\eta') + Au^2(\xi',\eta'), \end{aligned} \tag{63}$$

and

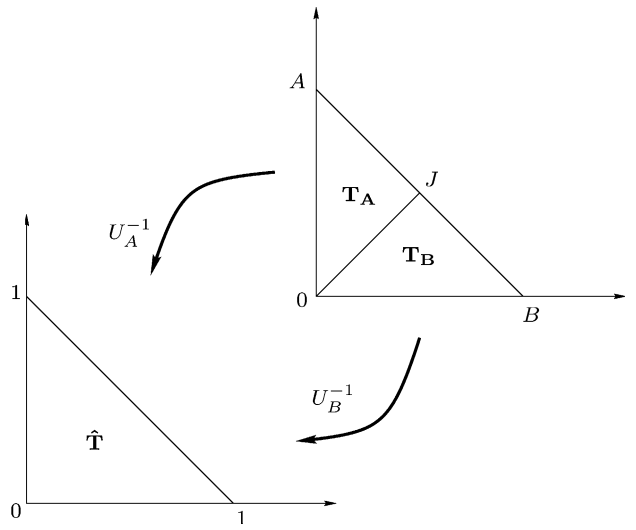

Fig. 11. Transformations mapping the triangles T_A and T_B to $\hat{T}$.

$$\begin{aligned} &U_B : \hat{T} \to T_B \\ &\quad (\xi',\eta') \mapsto U_B(\xi',\eta') = Ju^0(\xi',\eta') + Bu^2(\xi',\eta'), \end{aligned} \tag{64}$$

inducing two variable transformations, we have:

$$\int_{T_A} k(\xi,\eta)\,\mathrm{d}\xi\,\mathrm{d}\eta = |\hat{T}| \int_{\hat{T}} k \circ U_A(\xi',\eta')\,\mathrm{d}\xi'\,\mathrm{d}\eta', \tag{65}$$

and

$$\int_{T_B} k(\xi,\eta)\,\mathrm{d}\xi\,\mathrm{d}\eta = |\hat{T}| \int_{\hat{T}} k \circ U_B(\xi',\eta')\,\mathrm{d}\xi'\,\mathrm{d}\eta'. \tag{66}$$

Then, the two integrals above, being defined over the reference triangle, may be integrated by a Gauss–Hammer quadrature formula applied to the functions $k \circ U_A$ or $k \circ U_B$. The subdivision procedure may be continued until the wanted accuracy is reached. Thus, by iterating this process P times ($P \geqslant 1$), we get

$$K = K_P = |\hat{T}|^P \sum_{\Pi \in \mathscr{A}_P} \int_{\hat{T}} k \circ U_{\Pi(1)} \circ U_{\Pi(2)} \cdots \circ U_{\Pi(P)}(\xi_P^\Pi,\eta_P^\Pi)\,\mathrm{d}\xi_P^\Pi\,\mathrm{d}\eta_P^\Pi, \tag{67}$$

where $\mathscr{A}_P$ is the set of mappings from the set $\{1,\ldots,P\}$ to the set $\{A,B\}$ and $(\xi_n^\Pi,\eta_n^\Pi)_{n=1,\ldots,P}$ is the sequence of variables due to the variable transformations induced by a given $\Pi \in \mathscr{A}_P$. The relation between (ξ_n^Π,η_n^Π) and $(\xi_{n+1}^\Pi,\eta_{n+1}^\Pi)$ can be derived by writing the mappings U_A and U_B in a matrix form. Let us define for that purpose the following quantities:

$$M_A = \frac{1}{2}\begin{pmatrix} -1 & -1 \\ -1 & 1 \end{pmatrix},$$

$$M_B = \frac{1}{2}\begin{pmatrix} -1 & 1 \\ -1 & -1 \end{pmatrix},$$

$$Y = \frac{1}{2}\begin{pmatrix} 1 \\ 1 \end{pmatrix},$$

$$X_n^{\Pi} = \begin{pmatrix} \xi_n^{\Pi} \\ \eta_n^{\Pi} \end{pmatrix}.$$

Then from (63) and (64) we have:

$$X_n^{\Pi} = M_{\Pi(n+1)} X_{n+1}^{\Pi} + Y, \quad n = 0, \ldots, P-1, \qquad X_0^{\Pi} = \begin{pmatrix} \xi \\ \eta \end{pmatrix}. \tag{68}$$

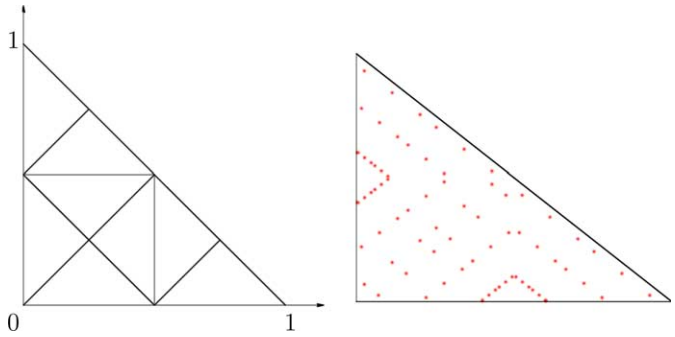

Fig. 12. Triangles and quadrature points distribution for $P = 2$, $N = 9$.

Table 1
Table showing the convergence of the subdivision method to the exact value

P	Semi-analytical value
0	2.850104132017379
1	2.845615828568151
2	2.841283391873457
3	2.839460514466428
4	2.838225797090046
5	2.837714948869154
6	2.837390629062305
7	2.837256027562511
8	2.837172989130881
9	2.837138477096164
10	2.837117472659868
11	2.837108736937710
12	2.837103455224714
13	2.837101257829896
14	2.837099933576150
15	2.837099382544410
16	2.837099051002786
17	2.837098913034472
18	2.837098830089292
19	2.837098795570917
Exact value	2.837098756400005

We deduce from the previous relation that

$$X_0^{\Pi} = M_n^{\Pi} X_n^{\Pi} + V_n^{\Pi}, \quad n = 0, \ldots, P, \tag{69}$$

where $(M_n^{\Pi})_{n=0,\ldots,P}$ and $(V_n^{\Pi})_{n=0,\ldots,P}$ are two sequences defined by:

$$M_{n+1}^{\Pi} = M_n^{\Pi} M_{\Pi(n+1)}, \quad n = 0, \ldots, P-1, \qquad M_0^{\Pi} = \begin{pmatrix} 1 & 0 \\ 0 & 1 \end{pmatrix}, \tag{70}$$

and

$$V_{n+1}^{\Pi} = M_n^{\Pi} Y + V_n^{\Pi}, \quad n = 0, \ldots, P-1, \qquad V_0^{\Pi} = \begin{pmatrix} 0 \\ 0 \end{pmatrix}. \tag{71}$$

Fig. 12 shows the distribution of the triangles and the quadrature points after $P = 2$ steps of the subdivision method.

5.2. Numerical experiment

We present below a numerical experiment showing the efficiency of the subdivision method, where the algorithm presented in the previous subsection has been implemented recursively. We consider the situation given by the Fig. 7 with $h = 0$ and $a = 1$. We compare the exact value computed by the expression (45) with

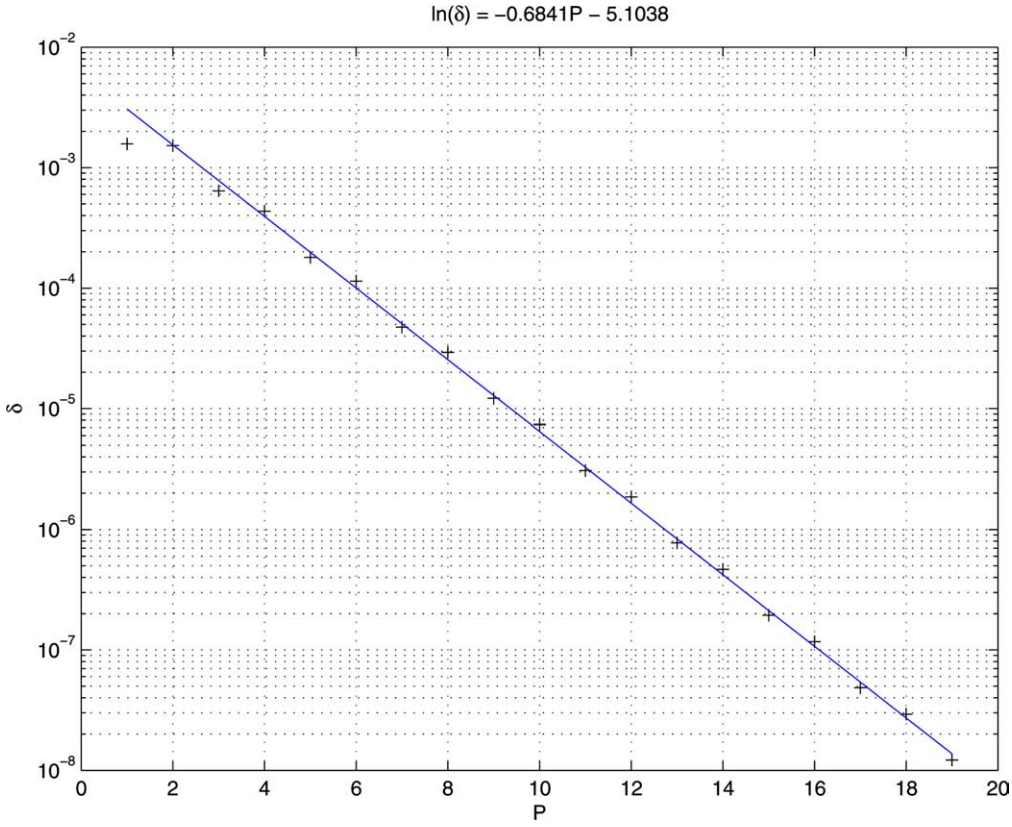

Fig. 13. Evolution of the discrepancy δ versus P.

$SAGH_9$ using the method described in the previous section. Table 1 shows the evolution of the value obtained by the semi-analytical method versus P, the number of subdivision steps, with 16 digits of precision. We may check when P increases that the precision increases too. The computed value tends to the exact one. Let us consider the discrepancy δ defined by:

$$\delta = \frac{|\tilde{K}_P - \tilde{K}_{P-1}|}{\tilde{K}_{P-1}}, \quad P = 1,2,3,\ldots, \tag{72}$$

where $\tilde{K}_P$ is an approximation of K_P obtained with numerical integration. The Fig. 13 shows the evolution of δ versus N. A linear interpolation yields that $\ln(\delta)$ may be considered as an affine function of P, $P \geqslant 2$, with a good approximation (see Fig. 13). $\delta < 10^{-q}$, q being an integer, means that q first digits of the numerical value are stabilized. Thus, although the relative error between $\tilde{K}_1$ and $\tilde{K}_0$ is about 0.16%, the graph shows that $10^{-3} < \delta < 10^{-2}$ meaning the two first digits are stabilized, which could not be enough for a given required precision. For $P = 19$, only eight digits are stabilized. Between each level, the computation time doubles. Extrapolating the relation between δ and P, we get that we should have $P = 47$ to get $q = 16$ digits stabilized, which corresponds to the machine double precision. However, the computation time becomes 2^{47} times the computation time for $P = 0$.

The computation time depends also on the platforms that are used to perform it and in the algorithmic methods (sequential or parallel computing). A sensitive advantage is that the method does not require mesh subdivision, as the triangle subdivision is included in the integration method. A compromise has to be found between the acceptable computation time and the accuracy required.

6. Conclusion

We derived in this paper a method allowing to calculate integrals of the kind I_1 and I_2^k without numerical singularities. This method requires the exact analytic calculation of double integrals. We have shown the efficiency of the method in removing these numerical singularities.

The developed semi-analytic method is not symmetric for the calculation of I_1, unlike the Gauss–Hammer quadrature. It depends on the triangle over which the exact integration is performed. The greater is the triangle, the greater is the error for a pure numerical integration with a given number of Gauss–Hammer points. Thus, since the method is hybrid one using a Gauss–Hammer quadrature combined with an exact integration, the exact integration must be done over the largest of the two triangles so as to achieve the best accuracy.

We presented a subdivision method allowing to improve this accuracy without requiring mesh subdivision. This method leads to a compromise between accuracy and calculation time requirements. It gives satisfactory results in the case of the electromagnetic problem which motivated this work.

Finally, we mention that a great part of this work has been done using Maple releases 6.0 to 8.0, aiming to put the different kernels on a form allowing formal integration.

References

[1] A. Bossavit, Electromagnétisme, en vue de la modélisation, Springer-Verlag, 1988.
[2] A. Bossavit, J.-C. Vérité, The trifou code: Solving the 3-d eddy-current problem using h as state variable, IEEE Trans. Magn. Mag-19 (6) (1983) 2465–2470.
[3] H. Brass, G. Hämerlin, in: Numerical Integration III Proceedings of the Conference, vol. ISNM 85, Birkhäuser Verlag, 1987.
[4] P.-A. Chevalier, Un Modèle Mathématique Pour L'Étude Des Courants De Foucault En Dimension, vol. 3, Department of Mathematics, Swiss Federal Institute of Technology, 1989.

[5] S. Clain, J. Rappaz, M. Swierkosz, R. Touzani, Numerical modeling of induction heating for two-dimensional geometries, M^3AS 3 (6) (1993) 805–822.
[6] Pasi Ylä-Oijala, Matti Taskinen, Calculation of CFIE impedance matrix elements with RWG and n × RWG functions, IEEE Trans. Antennas Propagation 51 (8) (2003) 1837–1846.
[7] Roberto D. Graglia, On the numerical integration of the linear shape functions times the 3-D Green's function or its gradient on a plane triangle, IEEE Trans. Antennas Propagation 41 (10) (1993) 1448–1455.
[8] Ph.J. Davis, Ph. Rabinowitz, Methods of numerical integration, Computer Science and Applied Mathematics, second ed., Academic Press, 1984.
[9] T.O. Espelid, A. Genz, Numerical integration recent developments, software and applications, NATO ASI Series C 357 (1992).
[10] G. Hämerlin, in: Numerical Integration Proceedings of the Conference, vol. ISNM 57, Birkhäuser Verlag, 1981.
[11] M. Mori, M. Sugihara, The double-exponential transformation in numerical analysis, J. Comput. Appl. Math. 127 (2001) 287–296.
[12] J.-C. Nédélec, Computation of eddy currents on a surface in $\mathbb{R}^3$ by finite element methods, SIAM J. Numer. Anal. 15 (1978) 580–594.
[13] J. Rappaz, M. Swierkosz, C. Trophime, Un Modèle Mathématique et Numérique pour un Logiciel de Simulation Tridimensionnelle d'Induction Electromagnétique, Department of Mathematics, Swiss Federal Institute of Technology, Internal Report, 1999.
[14] J.-C. Vérité, Trifou: un code de calcul tridimensionnel des courants de foucault, IEEE Trans. Magn. Mag-23 (3) (1987) 1881–1887.